

Periodic response analysis of a misaligned rotor system by harmonic balance method with alternating frequency/time domain technique

LI HongLiang^{1*}, CHEN YuShu¹, HOU Lei¹ & ZHANG ZhiYong²

¹ School of Astronautics, Harbin Institute of Technology, Harbin 150001, China;

² School of Science, Nanjing University of Science and Technology, Nanjing 210094, China

Received December 23, 2015; accepted May 10, 2016; published online August 16, 2016

A dynamic model is established for an offset-disc rotor system with a mechanical gear coupling, which takes into consideration the nonlinear restoring force of rotor support and the effect of coupling misalignment. Periodic solutions are obtained through harmonic balance method with alternating frequency/time domain (HB-AFT) technique, and then compared with the results of numerical simulation. Good agreement confirms the feasibility of HB-AFT scheme. Moreover, the Floquet theory is adopted to analyze motion stability of the system when rotor runs at different speed intervals. A simple strategy to determine the monodromy matrix is introduced and two ways towards instability are found for periodic solutions: the period doubling bifurcation and the secondary Hopf bifurcation. The results obtained will contribute to the global response analysis and dynamic optimal design of rotor systems.

rotor system, coupling misalignment, harmonic balance method with alternating frequency/time domain (HB-AFT) technique, Floquet theory, stability, bifurcation

Citation: Li H L, Chen Y S, Hou L, et al. Periodic response analysis of a misaligned rotor system by harmonic balance method with alternating frequency/time domain technique. *Sci China Tech Sci*, 2016, 59: 1717–1729, doi: 10.1007/s11431-016-6101-7

1 Introduction

Rotor misalignment is one of the most common faults in the operation of rotating machinery. As perfect alignment of the driving and driven shafts can never be achieved practically, the misalignment condition is virtually always present in the machine trains. Even if a perfect alignment is achieved initially, it will be impossible to maintain it during the machine operation due to various factors, such as thermal distortion, movement of foundation, asymmetry in the applied load, etc. Thus the problem of misalignment is of great concern to the designers and maintenance engineers who

focus on understanding and diagnosing rotor misalignment to avoid any failure or damage may arise.

Shaft misalignment causes reaction force to be generated from the coupling which is often a major cause of machine vibration. There has been wide coverage in the literature of rotor misalignment. Dewell and Mitchell [1] determined the expected vibration frequencies for a misaligned metallic-disc flexible coupling and showed experimentally all the predicted frequencies through real-time spectrum analysis. Sekhar and Prabhu [2] studied shaft misalignment in a rotor-bearing system with flexible gear coupling using high order finite element method. They recommended the 2X vibration response as the characteristic signature of misaligned rotor shafts. Xu and Marangoni [3,4] presented a theoretical research on a misaligned motor-flexible cou-

*Corresponding author (email: andypang141592@163.com)

pling-rotor system and modeled the misalignment effect analytically using the universal joint kinematics. The derived results indicated that coupling misalignment produces a frequency that is twice of the shaft rotating frequency, and the vibration response due to shaft misalignment largely affects the even multiples of running speed. Laboratory experiments were carried out to support their theory. Lee and Lee [5] developed a theoretical model of a misaligned rotor on ball bearings. Experimental results revealed that the rotor whirl orbit tends to collapse towards a straight line as angular misalignment increases. Li and Yu [6] investigated the nonlinearly coupled lateral and torsional vibrations of a rotor system with a misaligned gear coupling. Numerical results showed the even multiples of running speed in lateral vibration and the odd multiples of running speed in torsional vibration. Al-Hussain and Redmond [7] modeled the mechanical coupling in the form of a radially rigid joint with rotational stiffness and discovered the 1X lateral-torsional coupled vibration response for two Jeffcott rotors with parallel misalignment. Al-Hussain [8] presented a further study on the effect of angular misalignment upon the motion stability of two rigid rotors connected by a flexible mechanical coupling. Sinha et al. [9] proposed a technique to estimate both the rotor unbalance and shaft misalignment from the single machine run-down data. Lees [10] analyzed the effects of parallel misalignment in rigidly coupled rotors mounted on the linearized bearings. Bouaziz et al. [11–13] investigated the dynamic behaviors of a misaligned rotor device supported by two hydrodynamic journal bearings. The influence of angular misalignment was essentially characterized in frequency domain by the presence of two dominant peaks and the comparison between rolling bearing and hydrodynamic journal bearing also showed that hydrodynamic bearing permits to attenuate vibration due to the misalignment defect. A similar work was subsequently reported on a misaligned rotor system with active magnetic bearings. Patel and Darpe [14,15] analyzed the influence of various types of misalignment on the rotor vibration. A coupled rotor system in the bending, longitudinal and torsional modes was modeled by using finite element method based upon the Timoshenko beam theory. Experimental tests were then carried out to reveal the unique nature of misalignment fault leading to reliable misalignment diagnosis. Jalan and Mohanty [16] developed a model based technique for fault diagnosis of a rotor system with coupling misalignment and mass unbalance. The fault condition and location were successfully detected with the utilization of residual generation technique. Redmond [17] introduced a flexibly misaligned shaft model that incorporates both the angular and parallel misalignment in the presence of mass unbalance. A series of numerical simulations were performed on the dimensionless dynamical response to evaluate the influence of several key parameters. Rybczynski [18] showed a computer simulation of bearing misalignment defects in a power turbo-generator. The obtained results

indicated that bearing trajectories carry much important information on the position and direction of bearing dislocations which can be used to diagnose the misalignment fault in rotating machines. Lal and Tiwari [19,20] developed an identification algorithm to estimate the bearing and coupling parameters along with the mass unbalance parameters in a simplified turbine-generator model by using the forced response information. This algorithm based upon the least-squares fit technique was further extended to the multi-disc, multi-bearing and multi-coupling rotor systems and proved to be effective and robust. The automatic control of misaligned rotor systems gained an increasing attention from engineers. All the actual engineering systems are typical complex networks, and the rotor system is no exception. Investigation on the synchronization of complex networks is of great significance in the various science and engineering fields, such as cellular and metabolic networks, the Internet, social communities, electric power grids, multi-rotor engine systems, etc. These large-scale dynamic networks often display some synchronous behaviors among their constituents, and some rules about this phenomena were demonstrated in a time-varying dynamic network [21] and a specific duplex network [22] respectively. Liu et al. [23] utilized the delay-input and discretization approaches to design the sampled-data controllers for the robust consensus of the multi-agent systems. Two sufficient conditions were deduced to ensure the robust consensus of multi-agent systems with external noises and the estimates of convergence speed of consensus errors were obtained as well. Then Liu et al. [24] developed the finite-time consensus criteria for a class of multi-agent systems with nonlinear dynamics using adaptive technique. Unlike the traditional ones, the proposed controllers do not need the prior information on Lipschitz constants and eigenvalues of Laplacian matrix. The above control strategies in networks are also suitable for other engineering systems, especially misaligned rotor systems. On the other hand, the research on rotor systems [25,26] can be helpful for understanding the dynamical behaviors and topological structures of many real-world complex networks.

Even the problem of rotor misalignment has been widely discussed, not much work is focused on nonlinear dynamics of misaligned rotor systems. Other than the linear system, it is always difficult to obtain the analytical solution of rotor system with strong nonlinear terms, such as piecewise and fractional exponential nonlinearities. Particularly with the variation of some key parameters, the system may exhibit a series of complex nonlinear behaviors, such as the jump and hysteresis phenomena, bifurcation and chaos, etc. That can not be explained by the typical linear theory. Therefore, it is necessary to find an effective way for solving the problems. The traditional analytical methods, like the small parameter method, the averaging method and the multi-scale method, are effective for response study of weakly nonlinear systems. When strong nonlinear problems are encountered, the har-

monic balance method (HB) is often adopted. However, the calculation accuracy is hard to ensure [27,28]. Based on the classic HB method, some revisions of it, including the perturbation HB method [29], the multi-scale HB method [30] and the elliptic-function HB method [31] were proposed for certain kinds of nonlinear problems. But these methods are not widely used in the engineering field due to their inherent limitations. The incremental harmonic balance method (IHB) is currently widespread in analyzing the response properties of strong nonlinear systems. In 1981, Lau and Cheung [32] firstly proposed the IHB method by combination of the incremental approach and the harmonic balance method, then it was applied to solve various nonlinear problems in engineering. The IHB method is not only suitable for the smooth dynamics [33,34], but it could also be used to deal with the piecewise-linear issues in gear pairs [35,36] and hinge joints [37,38]. However, it has difficulties with solving piecewise-discontinuous problem [39] since the incremental equations are usually obtained by the Taylor series expansion. A semi-analytical method of the implicit harmonic balance analysis named harmonic balance method with alternating frequency/time domain (HB-AFT) technique was firstly proposed by Yamauchi [40] in 1983. Then this method was developed to be a complete solution strategy for the periodic response of dynamic system by Kim and Noah [41–43]. Groll and Ewins [44] presented a homotopy continuation algorithm together with HB-AFT technique to compute the hysteresis response. Tiwari and Gupta [45] applied the HB-AFT scheme to rotor-bearing systems to validate the steady response obtained by numerical integration. Villa et al. [46] reported a whole frequency domain analysis method based on the HB-AFT and perturbation technique. Zhang et al. [47,48] investigated the local resonance and global bifurcation chaos behaviors in varying compliance vibration of a ball bearing by HB-AFT method with arc-length continuation. The HB-AFT method establishes the relation of each order harmonic term directly from the discrete time frequency features, and there is little integration work required during the solving process. Thus, the HB-AFT method is considered to be more versatile for strong nonlinear systems with the piecewise and fractional exponential properties.

When the nonlinear restoring force of rotor supports and the effect of coupling misalignment are taken into consideration, motion equation of the rotor system possesses strong nonlinear properties and it is difficult to solve the equation analytically. In this case, numerical integration methods are often used to obtain the dynamic response of rotor systems. However, the mechanism of instability and bifurcation can not be revealed via numerical simulation. Thus this paper is mainly devoted to nonlinear mechanism analysis of a misaligned rotor system with the help of an improved harmonic balance method and the Floquet theory.

In this paper, a misaligned rotor system is studied when it is subjected to both unbalance and misalignment forces. The derived governing equation is solved with HB-AFT method

and the periodic response is obtained. Then motion stability is deeply investigated by using the Floquet theory and some observations on the system dynamic behaviors are given.

2 Physical model and governing equation

2.1 Misaligned rotor model

The analytical model is comprised of an electric motor and an offset-disc rotor that are connected by a mechanical gear coupling as shown in Figure 1. The rotor is mounted on ball bearings and driven at different speeds. The gear coupling is modeled of angular or parallel misalignment and the bearing clearance is considered in ball bearing close to the coupling because it suffers more severe wear and vibration under the alternating force generated from the coupling misalignment. Besides, the gyroscopic effects of rotor can not be neglected due to the lateral asymmetric rotor and support structures.

2.2 Reaction force due to coupling misalignment

Misalignment in gear coupling includes the angular, parallel and combined conditions as shown in Figure 2(b)–(d). The coupling consists of two half parts, each with the driving and driven shaft connection. The two half-couplings rotate around their axial center lines and engage with the shell separately. The shell is forced to revolve around both center lines of half-couplings during a whirl process and its center of cross section may move along a planar circle.

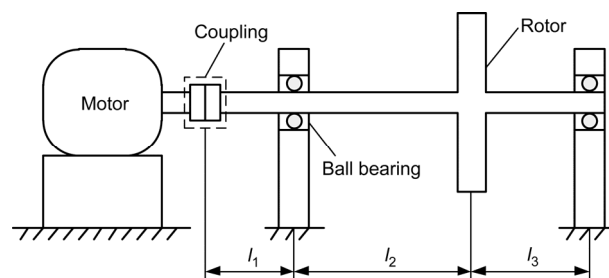


Figure 1 Schematic of the misaligned rotor system.

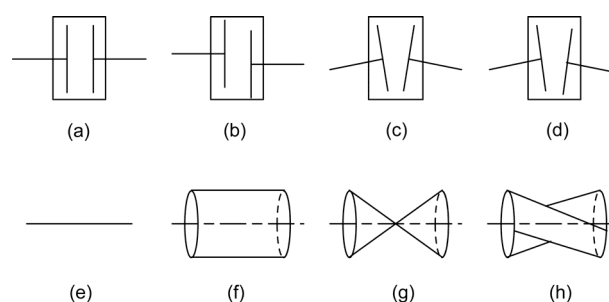


Figure 2 Misalignment and the corresponding motion conditions. (a) The alignment; (b) the parallel misalignment; (c) the angular misalignment; (d) the combined misalignment; (e) the straight line; (f) the cylindrical surface; (g) the double-cone surface; (h) the hemi double-cone surface.

According to the research of Han [49], central axis of the shell moves along a cylindrical surface when the coupling works with parallel misalignment. When angular misalignment appears in the coupling, central axis of the shell spins and swings continuously between two half-couplings and its motion trace is a double-cone surface. If the coupling works with both the angular and parallel misalignment, the central axis trace of the shell is a hemi double-cone surface which is a situation between cylindrical and double-cone surfaces. Different motion styles of the shell in various misalignment conditions are shown in Figure 2(f), (g) and (h).

Figure 3 gives the motion trace of the shell center, where o is the static center of the shell, o' is the dynamic center of the shell, o_1 and o_2 are the centers of two half-couplings, ω is the rotating speed of rotor, ϕ is the initial angle, ω' is the revolution speed of the shell, Δe is the equivalent amount of misalignment. For the parallel misalignment Δy , $\Delta e = \Delta y$. For the angular misalignment $\Delta \alpha$, $\Delta e = L \tan(\Delta \alpha / 2)$, where L is the assemble distance between two half-couplings.

The motion trace of the shell center can be expressed as

$$\begin{cases} x = \frac{\Delta e}{2} \cos(\omega't + \phi') = \frac{\Delta e}{2} \cos(2\omega t + 2\phi), \\ y = \frac{\Delta e}{2} \sin(\omega't + \phi') = \frac{\Delta e}{2} \sin(2\omega t + 2\phi). \end{cases} \quad (1)$$

When the half-couplings rotate around their center lines with the speed ω , the shell center revolves around its static position with a speed which is twice of ω . Since the shell always has a large mass, its motion virtually means applying an inertial centrifugal force on the rotor system.

The inertial centrifugal force can be obtained

$$\begin{cases} F_x = -M\ddot{x} = 2\Delta e M \omega^2 \cos(2\omega t + 2\phi), \\ F_y = -M\ddot{y} = 2\Delta e M \omega^2 \sin(2\omega t + 2\phi), \end{cases} \quad (2)$$

where M is the mass of the shell.

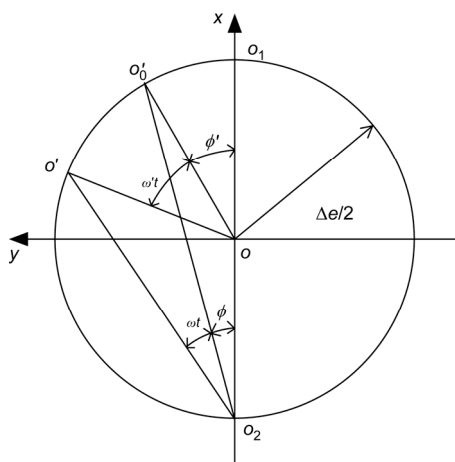


Figure 3 Motion trace of the shell center.

2.3 Rotor support force and dynamic equation

Bearing clearance and the nonlinear contacting stiffness are considered in the bearing model as shown in Figure 4. The bearing is assumed to be isotropic because its deformation resistivity can be treated equivalent in each radial direction. It gives more intuitive understanding that the ball bearing is simplified to be axisymmetric by neglecting the distribution of balls in races.

Due to the point contact between the ball and race in ball bearing, the following relationship can be obtained through Hertz contact theory [50]

$$F = k\gamma^{\frac{3}{2}}, \quad (3)$$

where F is the applied load, γ is the elastic deformation, k is the contact stiffness.

Thus, the rotor support force can be expressed as [51]

$$F_r = \begin{cases} 0, & r \leq \delta, \\ k_b (r - \delta)^{\frac{3}{2}}, & r > \delta, \end{cases} \quad (4)$$

where r is the radial displacement of shaft, δ is the bearing clearance, k_b is the bearing stiffness.

It is assumed that x and y are translational displacements of rotor centroid, θ_x and θ_y are the rotational displacements of rotor shaft. Taking into account the gyroscopic effects of rotor, motion equation for the system can be written as

$$\begin{cases} m\ddot{x} + c_r \dot{x} + f_{x1} + f_{x2} \\ = \Delta e M \omega^2 \cos(2\omega t + 2\phi) + m e \omega^2 \cos(\omega t + \phi) - mg, \\ m\ddot{y} + c_l \dot{y} + f_{y1} + f_{y2} \\ = \Delta e M \omega^2 \sin(2\omega t + 2\phi) + m e \omega^2 \sin(\omega t + \phi), \\ J_d \ddot{\theta}_x + c_\theta \dot{\theta}_x + \omega J_p \dot{\theta}_y + f_{y1} l_2 - f_{y2} l_3 \\ = (l_1 + l_2) \Delta e M \omega^2 \sin(2\omega t + 2\phi), \\ J_d \ddot{\theta}_y + c_\theta \dot{\theta}_y - \omega J_p \dot{\theta}_x - f_{x1} l_2 + f_{x2} l_3 \\ = -(l_1 + l_2) \Delta e M \omega^2 \cos(2\omega t + 2\phi), \end{cases} \quad (5)$$

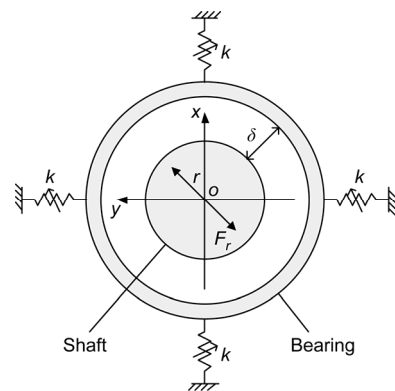


Figure 4 Simplified bearing model.

where m is the mass of rotor, J_d is the diametric moment of inertia of rotor, J_p is the polar moment of inertia of rotor, M is the mass of coupling shell, c_l and c_θ are the damping coefficients, f_{x1} and f_{y1} are the left bearing force components, f_{x2} and f_{y2} are the right bearing force components, Δe is the equivalent amount of misalignment, e is the eccentricity of rotor, ω is the speed of rotor, l_1 , l_2 and l_3 are the dimensions of rotor system shown in Figure 1, g is the acceleration of gravity, ϕ is the initial eccentric angle.

According to eq. (4), f_{x1} and f_{y1} can be expressed as

$$\begin{cases} f_{x1} = c_b \dot{x}_1 + k_b (r_1 - \delta)^{\frac{3}{2}} \frac{x_1}{r_1} H(r_1 - \delta), \\ f_{y1} = c_b \dot{y}_1 + k_b (r_1 - \delta)^{\frac{3}{2}} \frac{y_1}{r_1} H(r_1 - \delta), \end{cases} \quad r_1 = \sqrt{x_1^2 + y_1^2}, \quad (6)$$

where x_1 and y_1 are the displacements of rotor shaft at the left bearing, $H(q)$ is the Heaviside function.

$$H(q) = \begin{cases} 0, & q \leq 0, \\ 1, & q > 0. \end{cases} \quad (7)$$

Based on the kinematic analysis of rotor, x_1 and y_1 are

$$\begin{cases} x_1 = x - l_2 \theta_y, \\ y_1 = y + l_2 \theta_x. \end{cases} \quad (8)$$

In the same way, f_{x2} and f_{y2} can be expressed as

$$\begin{cases} f_{x2} = c_b \dot{x}_2 + k_b x_2 \sqrt{r_2}, \\ f_{y2} = c_b \dot{y}_2 + k_b y_2 \sqrt{r_2}, \end{cases} \quad r_2 = \sqrt{x_2^2 + y_2^2}, \quad (9)$$

where x_2 and y_2 are the displacements of rotor shaft at the right bearing, c_b is the bearing damping.

Then x_2 and y_2 are given by

$$\begin{cases} x_2 = x + l_3 \theta_y, \\ y_2 = y - l_3 \theta_x. \end{cases} \quad (10)$$

To give eq. (5) a dimensionless form, it can be assumed

$$\begin{aligned} \bar{x} &= x/e, \quad \bar{y} = y/e, \quad \bar{l}_1 = l_1/e, \quad \bar{l}_2 = l_2/e, \\ \bar{l}_3 &= l_3/e, \quad \Delta \bar{e} = \Delta e/e, \quad \bar{\delta} = \delta/e, \quad \tau = \omega t, \\ a &= Me^2/J_d, \quad b = me^2/J_d, \quad J = J_p/J_d, \\ p &= a\Delta \bar{e}/b, \quad q = a\Delta \bar{e}(\bar{l}_1 + \bar{l}_2), \quad \bar{g} = g/e\omega^2, \end{aligned} \quad (11)$$

then eq. (5) becomes

$$\begin{cases} \ddot{\bar{x}} + \ddot{\bar{f}}_{x1} + \ddot{\bar{f}}_{x2} = p \cos(2\tau + 2\phi) + \cos(\tau + \phi) - \bar{g}, \\ \ddot{\bar{y}} + \ddot{\bar{f}}_{y1} + \ddot{\bar{f}}_{y2} = p \sin(2\tau + 2\phi) + \sin(\tau + \phi), \\ \theta_x'' + J\theta_x' + \ddot{\bar{f}}_{y1}\bar{l}_2b - \ddot{\bar{f}}_{y2}\bar{l}_3b = q \sin(2\tau + 2\phi), \\ \theta_y'' - J\theta_y' - \ddot{\bar{f}}_{x1}\bar{l}_2b + \ddot{\bar{f}}_{x2}\bar{l}_3b = -q \cos(2\tau + 2\phi), \end{cases} \quad (12)$$

where ' denotes the derivative with respect to τ .

3 HB-AFT scheme and stability analysis

3.1 HB-AFT scheme

Since eq. (12) is a nonlinear dynamic equation with piecewise and fractional exponential properties, it is difficult to solve it analytically. Thus the HB-AFT scheme is employed.

For convenience, the variables are redefined as

$$X = \bar{x}, \quad Y = \bar{y}, \quad Z = \theta_x, \quad W = \theta_y, \quad (13)$$

then, eq. (12) is transformed into the matrix form

$$U'' + CU' + F = D, \quad (14)$$

where

$$U = [X \ Y \ Z \ W]^T, \quad F = [F_x \ F_y \ F_z \ F_w]^T, \quad D = [D_x \ D_y \ D_z \ D_w]^T, \quad (15)$$

$$C = \begin{bmatrix} \frac{2c_b}{m\omega} & 0 & 0 & \frac{c_b}{m\omega}(\bar{l}_3 - \bar{l}_2) \\ 0 & \frac{2c_b}{m\omega} & \frac{c_b}{m\omega}(\bar{l}_2 - \bar{l}_3) & 0 \\ 0 & \frac{c_b b}{m\omega}(\bar{l}_2 - \bar{l}_3) & \frac{c_b b}{m\omega}(\bar{l}_2^2 + \bar{l}_3^2) & J \\ \frac{c_b b}{m\omega}(\bar{l}_3 - \bar{l}_2) & 0 & -J & \frac{c_b b}{m\omega}(\bar{l}_2^2 + \bar{l}_3^2) \end{bmatrix}.$$

According to eq. (12), F_x , F_y , F_z and F_w are given by

$$\begin{aligned} F_x &= \frac{k_b \sqrt{e}}{m\omega^2} \frac{X - \bar{l}_2 W}{R_1} (R_1 - \bar{\delta})^{\frac{3}{2}} H(R_1 - \bar{\delta}) \\ &\quad + \frac{k_b \sqrt{e}}{m\omega^2} (X + \bar{l}_3 W) \sqrt{R_2}, \\ F_y &= \frac{k_b \sqrt{e}}{m\omega^2} \frac{Y + \bar{l}_2 Z}{R_1} (R_1 - \bar{\delta})^{\frac{3}{2}} H(R_1 - \bar{\delta}) \\ &\quad + \frac{k_b \sqrt{e}}{m\omega^2} (Y - \bar{l}_3 Z) \sqrt{R_2}, \\ F_z &= \frac{k_b \sqrt{e}}{m\omega^2} \frac{Y + \bar{l}_2 Z}{R_1} (R_1 - \bar{\delta})^{\frac{3}{2}} H(R_1 - \bar{\delta}) b \bar{l}_2 \\ &\quad - b \bar{l}_3 \frac{k_b \sqrt{e}}{m\omega^2} (Y - \bar{l}_3 Z) \sqrt{R_2}, \\ F_w &= \frac{k_b \sqrt{e}}{m\omega^2} \frac{X - \bar{l}_2 W}{R_1} (R_1 - \bar{\delta})^{\frac{3}{2}} H(R_1 - \bar{\delta}) (-b \bar{l}_2) \\ &\quad + b \bar{l}_3 \frac{k_b \sqrt{e}}{m\omega^2} (X + \bar{l}_3 W) \sqrt{R_2}, \end{aligned} \quad (16)$$

where

$$\begin{aligned}
 R_1 &= \sqrt{(X - \bar{l}_2 W)^2 + (Y + \bar{l}_2 Z)^2}, \\
 R_2 &= \sqrt{(X + \bar{l}_3 W)^2 + (Y - \bar{l}_3 Z)^2},
 \end{aligned}
 \tag{17}$$

then D_X, D_Y, D_Z and D_W are given by

$$\begin{aligned}
 D_X &= p \cos(2\tau + 2\phi) + \cos(\tau + \phi) - \bar{g}, \\
 D_Y &= p \sin(2\tau + 2\phi) + \sin(\tau + \phi), \\
 D_Z &= q \sin(2\tau + 2\phi), \quad D_W = -q \cos(2\tau + 2\phi).
 \end{aligned}
 \tag{18}$$

The periodic solution of eq. (14) can be represented as

$$\begin{bmatrix} X \\ Y \\ Z \\ W \end{bmatrix} = \begin{bmatrix} a_{X0} \\ a_{Y0} \\ a_{Z0} \\ a_{W0} \end{bmatrix} + \sum_{k=1}^K \left\{ \begin{bmatrix} a_{Xk} \\ a_{Yk} \\ a_{Zk} \\ a_{Wk} \end{bmatrix} \cos(k\tau) - \begin{bmatrix} b_{Xk} \\ b_{Yk} \\ b_{Zk} \\ b_{Wk} \end{bmatrix} \sin(k\tau) \right\}, \tag{19}$$

where a_{X0}, a_{Y0}, a_{Z0} and a_{W0} are the constants, a_{Xk}, a_{Yk}, a_{Zk} and a_{Wk} are the coefficients of cosine terms, b_{Xk}, b_{Yk}, b_{Zk} and b_{Wk} are the coefficients of sine terms, K is the maximum number of the considered harmonic terms.

Similarly, the nonlinear restoring force can be written as

$$\begin{bmatrix} F_X \\ F_Y \\ F_Z \\ F_W \end{bmatrix} = \begin{bmatrix} c_{X0} \\ c_{Y0} \\ c_{Z0} \\ c_{W0} \end{bmatrix} + \sum_{k=1}^K \left\{ \begin{bmatrix} c_{Xk} \\ c_{Yk} \\ c_{Zk} \\ c_{Wk} \end{bmatrix} \cos(k\tau) - \begin{bmatrix} d_{Xk} \\ d_{Yk} \\ d_{Zk} \\ d_{Wk} \end{bmatrix} \sin(k\tau) \right\}, \tag{20}$$

where c_{X0}, c_{Y0}, c_{Z0} and c_{W0} are the constants, c_{Xk}, c_{Yk}, c_{Zk} and c_{Wk} are the coefficients of cosine terms, d_{Xk}, d_{Yk}, d_{Zk} and d_{Wk} are the coefficients of sine terms, K is the maximum number of the considered harmonic terms.

Substituting eqs. (19) and (20) into eq. (14) and balancing the coefficients of harmonic terms in each order, the following algebraic equations G_s are obtained.

For the constant terms,

$$\begin{bmatrix} G(1) \\ G(2) \\ G(3) \\ G(4) \end{bmatrix} = \begin{bmatrix} c_{X0} \\ c_{Y0} \\ c_{Z0} \\ c_{W0} \end{bmatrix} + \begin{bmatrix} \bar{g} \\ 0 \\ 0 \\ 0 \end{bmatrix} = 0, \tag{21}$$

for the cosine terms,

$$\begin{bmatrix} G(8k-3) \\ G(8k-2) \\ G(8k-1) \\ G(8k) \end{bmatrix} = k^2 \begin{bmatrix} a_{Xk} \\ a_{Yk} \\ a_{Zk} \\ a_{Wk} \end{bmatrix} + kC \begin{bmatrix} b_{Xk} \\ b_{Yk} \\ b_{Zk} \\ b_{Wk} \end{bmatrix} - \begin{bmatrix} c_{Xk} \\ c_{Yk} \\ c_{Zk} \\ c_{Wk} \end{bmatrix} + \begin{bmatrix} p\phi_2 + \phi_1 \\ 0 \\ 0 \\ -q\phi_2 \end{bmatrix} = 0, \tag{22}$$

for the sine terms,

$$\begin{bmatrix} G(8k+1) \\ G(8k+2) \\ G(8k+3) \\ G(8k+4) \end{bmatrix} = kC \begin{bmatrix} a_{Xk} \\ a_{Yk} \\ a_{Zk} \\ a_{Wk} \end{bmatrix} - k^2 \begin{bmatrix} b_{Xk} \\ b_{Yk} \\ b_{Zk} \\ b_{Wk} \end{bmatrix} + \begin{bmatrix} d_{Xk} \\ d_{Yk} \\ d_{Zk} \\ d_{Wk} \end{bmatrix} + \begin{bmatrix} 0 \\ p\phi_2 + \phi_1 \\ q\phi_2 \\ 0 \end{bmatrix} = 0, \tag{23}$$

where

$$\phi_1 = \begin{cases} 0, & k \neq 1, \\ 1, & k = 1, \end{cases} \quad \phi_2 = \begin{cases} 0, & k \neq 2, \\ 1, & k = 2, \end{cases} \quad k = 1, 2, \dots, K. \tag{24}$$

The desired periodic solution can be obtained by solving eqs. (21)–(23) that are implicit algebraic equations hard to be solved directly. Thus a Newton-Raphson iteration procedure is adopted. Let

$$\begin{aligned}
 \mathbf{P} &= [a_{X0} \ a_{Y0} \ a_{Z0} \ a_{W0} \ a_{X1} \ a_{Y1} \ a_{Z1} \ a_{W1} \ b_{X1} \ b_{Y1} \ b_{Z1} \ b_{W1} \\
 &\quad \dots \ a_{XK} \ a_{YK} \ a_{ZK} \ a_{WK} \ b_{XK} \ b_{YK} \ b_{ZK} \ b_{WK}]^T, \\
 \mathbf{Q} &= [c_{X0} \ c_{Y0} \ c_{Z0} \ c_{W0} \ c_{X1} \ c_{Y1} \ c_{Z1} \ c_{W1} \ d_{X1} \ d_{Y1} \ d_{Z1} \ d_{W1} \\
 &\quad \dots \ c_{XK} \ c_{YK} \ c_{ZK} \ c_{WK} \ d_{XK} \ d_{YK} \ d_{ZK} \ d_{WK}]^T.
 \end{aligned}
 \tag{25}$$

Taking \mathbf{P} as an unknown variable, the fix point \mathbf{P}^* can be found from an initial guess \mathbf{P}^0 through the Newton-Raphson iteration procedure for eqs. (21)–(23). That is

$$\mathbf{J}^{(i)} (\mathbf{P}^{(i+1)} - \mathbf{P}^{(i)}) + \mathbf{G}^{(i)} = 0, \tag{26}$$

where \mathbf{J} is the Jacobian matrix, i.e. $\mathbf{J} = d\mathbf{G}/d\mathbf{P}$.

The values of \mathbf{Q}, \mathbf{G} and \mathbf{J} in each step of iterations can be obtained by an alternating frequency/time domain technique. For a supposed \mathbf{P} , the discrete values of X, Y, Z, W in time domain are given by the inverse discrete Fourier transform

$$\begin{bmatrix} X(n) \\ Y(n) \\ Z(n) \\ W(n) \end{bmatrix} = \begin{bmatrix} a_{X0} \\ a_{Y0} \\ a_{Z0} \\ a_{W0} \end{bmatrix} + \sum_{k=1}^K \left\{ \begin{bmatrix} a_{Xk} \\ a_{Yk} \\ a_{Zk} \\ a_{Wk} \end{bmatrix} \cos \frac{2\pi kn}{N} - \begin{bmatrix} b_{Xk} \\ b_{Yk} \\ b_{Zk} \\ b_{Wk} \end{bmatrix} \sin \frac{2\pi kn}{N} \right\}, \tag{27}$$

where N is the number of samples in a period, $n=0,1, \dots, N-1$.

According to eqs. (16) and (27), the discrete values of F_X, F_Y, F_Z and F_W can be obtained

$$\begin{bmatrix} F_X(n) \\ F_Y(n) \\ F_Z(n) \\ F_W(n) \end{bmatrix} = \begin{bmatrix} F_X(X(n), Y(n), Z(n), W(n)) \\ F_Y(X(n), Y(n), Z(n), W(n)) \\ F_Z(X(n), Y(n), Z(n), W(n)) \\ F_W(X(n), Y(n), Z(n), W(n)) \end{bmatrix}, \tag{28}$$

then, the discrete values of F_X, F_Y, F_Z and F_W in frequency domain are given as \mathbf{Q} by the discrete Fourier transform

$$\begin{bmatrix} c_{X0} \\ c_{Y0} \\ c_{Z0} \\ c_{W0} \end{bmatrix} = \frac{1}{N} \sum_{n=0}^{N-1} \begin{bmatrix} F_X(n) \\ F_Y(n) \\ F_Z(n) \\ F_W(n) \end{bmatrix},$$

$$\begin{bmatrix} c_{Xk} \\ c_{Yk} \\ c_{Zk} \\ c_{Wk} \end{bmatrix} = \frac{2}{N} \sum_{n=0}^{N-1} \begin{bmatrix} F_X(n) \\ F_Y(n) \\ F_Z(n) \\ F_W(n) \end{bmatrix} \cos \frac{2\pi kn}{N}, \tag{29}$$

$$\begin{bmatrix} d_{Xk} \\ d_{Yk} \\ d_{Zk} \\ d_{Wk} \end{bmatrix} = -\frac{2}{N} \sum_{n=0}^{N-1} \begin{bmatrix} F_X(n) \\ F_Y(n) \\ F_Z(n) \\ F_W(n) \end{bmatrix} \sin \frac{2\pi kn}{N},$$

where $k=1,2,\dots,K$.

To calculate the derivatives in \mathbf{J} , eqs. (27)–(29) are utilized to yield

$$\begin{cases} \frac{\partial c_{\alpha 0}}{\partial a_{\beta 0}} = \frac{1}{N} \sum_{n=0}^{N-1} f_{\alpha\beta}(n), \\ \frac{\partial c_{\alpha 0}}{\partial a_{\beta j}} = \frac{1}{N} \sum_{n=0}^{N-1} f_{\alpha\beta}(n) \cos \frac{2\pi jn}{N}, \\ \frac{\partial c_{\alpha 0}}{\partial b_{\beta j}} = -\frac{1}{N} \sum_{n=0}^{N-1} f_{\alpha\beta}(n) \sin \frac{2\pi jn}{N}, \\ \frac{\partial c_{\alpha k}}{\partial a_{\beta 0}} = \frac{2}{N} \sum_{n=0}^{N-1} f_{\alpha\beta}(n) \cos \frac{2\pi kn}{N}, \\ \frac{\partial c_{\alpha k}}{\partial a_{\beta j}} = \frac{2}{N} \sum_{n=0}^{N-1} f_{\alpha\beta}(n) \cos \frac{2\pi jn}{N} \cos \frac{2\pi kn}{N}, \\ \frac{\partial c_{\alpha k}}{\partial b_{\beta j}} = -\frac{2}{N} \sum_{n=0}^{N-1} f_{\alpha\beta}(n) \sin \frac{2\pi jn}{N} \cos \frac{2\pi kn}{N}, \\ \frac{\partial d_{\alpha k}}{\partial a_{\beta 0}} = -\frac{2}{N} \sum_{n=0}^{N-1} f_{\alpha\beta}(n) \sin \frac{2\pi kn}{N}, \\ \frac{\partial d_{\alpha k}}{\partial a_{\beta j}} = -\frac{2}{N} \sum_{n=0}^{N-1} f_{\alpha\beta}(n) \cos \frac{2\pi jn}{N} \sin \frac{2\pi kn}{N}, \\ \frac{\partial d_{\alpha k}}{\partial b_{\beta j}} = \frac{2}{N} \sum_{n=0}^{N-1} f_{\alpha\beta}(n) \sin \frac{2\pi jn}{N} \sin \frac{2\pi kn}{N}, \end{cases} \tag{30}$$

where $j, k=1,2,\dots,K$,

$$f_{\alpha\beta}(n) = \frac{\partial F_{\alpha}(n)}{\partial \beta(n)}, \quad \alpha, \beta = X, Y, Z, W. \tag{31}$$

To get a desired periodic solution, \mathbf{P}^* can be determined in proper accuracy through an iteration procedure utilizing eq. (26) as follows.

(1) With an initial guess $\mathbf{P}^{(0)}$, calculate $\mathbf{Q}^{(0)}$ and $\mathbf{J}^{(0)}$ by using eqs. (27), (29) and (30).

(2) Iterate eq. (26) once, and get $\mathbf{P}^{(1)}$.

(3) Continue (1) and (2) until the iteration converges to \mathbf{P}^* which is accurate within an allowed error tolerance.

Multiple solutions may appear in some conditions. With the different initial guess, the iteration will trace a different path. Thus proper initial guessed values are the key points.

3.2 Stability analysis

Periodic solutions of the system can be obtained by using the HB-AFT method and their stability will be checked with the Floquet theory for bifurcation analysis. Let

$$\mathbf{V} = [\mathbf{U} \ \mathbf{U}']^T, \tag{32}$$

then eq. (14) is transformed into

$$\mathbf{V}' = \mathbf{F}(\tau, \mathbf{V}(\tau), \mu), \tag{33}$$

where μ is the bifurcation parameter.

It is assumed that eq. (33) has a periodic solution

$$\mathbf{V}^*(\tau) = \mathbf{V}^*(\tau + T), \tag{34}$$

\mathbf{v} is given to perturb the assumed periodic solution \mathbf{V}^* and the perturbed equation is obtained

$$(\mathbf{V}^* + \mathbf{v})' = \mathbf{F}(\tau, \mathbf{V}^* + \mathbf{v}, \mu), \tag{35}$$

then \mathbf{F} is dealt with the Taylor series expansion at \mathbf{V}^* and the linear terms are kept for eq. (35)

$$\mathbf{v}' = \frac{\partial \mathbf{F}}{\partial \mathbf{V}^*} \mathbf{v} = \mathbf{A}(\tau) \mathbf{v}, \tag{36}$$

where \mathbf{A} is a Jacobian matrix whose varying period is T .

Thus, the stability of \mathbf{V}^* depends on \mathbf{v} in eq. (36) which is a set of first-order time-varying differential equations. If the zero solution of \mathbf{v} is stable, \mathbf{V}^* is stable. Otherwise, \mathbf{V}^* is unstable. It is further elaborated as follows.

If $\mathbf{S}(\tau)$ is a fundamental solution of eq. (36), $\mathbf{S}(\tau + T)$ is the fundamental solution as well since $\mathbf{A}(\tau) = \mathbf{A}(\tau + T)$. The relation between $\mathbf{S}(\tau)$ and $\mathbf{S}(\tau + T)$ can be expressed as

$$\mathbf{S}(\tau) \mathbf{M} = \mathbf{S}(\tau + T). \tag{37}$$

It is assumed that the initial condition $\mathbf{S}(0) = \mathbf{I}$ is satisfied, \mathbf{I} is the identity matrix, therefore

$$\mathbf{M} = \mathbf{S}(T), \tag{38}$$

where \mathbf{M} is called the monodromy matrix. Its eigenvalues are the Floquet multipliers.

The Floquet multipliers can determine the stability of \mathbf{V}^* . If all Floquet multipliers are within the unit circle centered at the origin of the complex plane, \mathbf{V}^* is stable. Otherwise, \mathbf{V}^* is unstable and bifurcation will occur in three ways.

(1) If a Floquet multiplier leaves the unit circle through +1, the transcritical, symmetry-breaking or cyclic-folding bifurcation may occur.

(2) If a Floquet multiplier leaves the unit circle through -1, the period-doubling bifurcation occurs.

(3) If two complex conjugate Floquet multipliers move out of the unit circle away from the real axis, the secondary Hopf bifurcation occurs.

According to Hsu method, the approximate monodromy matrix can be expressed as [52]

$$M = \prod_{n=N}^1 \exp(A_n \Delta T) = \prod_{n=N}^1 \left[I + \sum_{j=1}^{N_j} \frac{(A_n \Delta T)^j}{j!} \right], \quad (39)$$

where N_j denotes the number of terms in the approximation of the constant matrix A_n exponential. It is reasonable to replace the time-varying matrix $A(\tau)$ by using the following constant matrix A_n in the n th time interval provided that N is chosen to be sufficiently large, ΔT denotes the time interval equally divided in a period.

The constant matrix A_n is given by

$$A_n = \frac{1}{\Delta T} \int_{\tau_{n-1}}^{\tau_n} A(\tau) d\tau, \quad (40)$$

where

$$\tau_n = n\Delta T = nT/N, \quad n = 1, 2, \dots, N. \quad (41)$$

Therefore, if the periodic solution of eq. (34) is obtained by the HB-AFT method, the desired monodromy matrix and the associated Floquet multipliers can be calculated according to eq. (39). Consequently, the stability and bifurcations of the periodic solutions can be investigated.

4 Computation results and discussion

The initial parameters of the system used for computation are as follows:

$$\begin{aligned} m &= 12.5 \text{ kg}, \quad M = 0.5 \text{ kg}, \quad J_p = 0.06 \text{ kg m}^2, \quad J_d = 0.03 \text{ kg m}^2, \\ l_1 &= 0.1 \text{ m}, \quad l_2 = 0.2 \text{ m}, \quad l_3 = 0.1 \text{ m}, \quad e = 2 \times 10^{-5} \text{ m}, \quad \delta = 2 \times 10^{-6} \text{ m}, \\ \Delta e &= 2 \times 10^{-4} \text{ m}, \quad c_b = 200 \text{ Ns/m}, \quad k_b = 7.055 \times 10^9 \text{ N/m}^{3/2}. \end{aligned}$$

When $\omega = 150$ rad/s, $K=8$, $N=256$ and the allowed error tolerance $\varepsilon = 10^{-12}$, the periodic solution obtained by the HB-AFT scheme is (higher harmonic terms are omitted here)

$$\begin{aligned} X &= -0.2408 + 0.0070 \cos(\tau) + 9.5906 \times 10^{-6} \sin(\tau) \\ &\quad + 0.0016 \cos(2\tau) + 5.8243 \times 10^{-6} \sin(2\tau) \\ &\quad - 3.6093 \times 10^{-5} \cos(3\tau) - 6.2967 \times 10^{-7} \sin(3\tau) \\ &\quad - 3.8057 \times 10^{-5} \cos(4\tau) - 8.7405 \times 10^{-7} \sin(4\tau), \\ Y &= -4.0735 \times 10^{-7} - 2.5610 \times 10^{-5} \cos(\tau) + 0.0112 \sin(\tau) \\ &\quad - 2.9119 \times 10^{-5} \cos(2\tau) + 0.0039 \sin(2\tau) \\ &\quad - 2.0396 \times 10^{-6} \cos(3\tau) + 1.0722 \times 10^{-4} \sin(3\tau) \\ &\quad - 2.9341 \times 10^{-6} \cos(4\tau) + 1.2248 \times 10^{-4} \sin(4\tau). \end{aligned}$$

As illustrated in Figure 5, the HB-AFT results agree well with the numerical solutions obtained by the Runge-Kutta

method. The calculation of the HB-AFT scheme possesses fast convergence speed and large convergent domain, which can be observed in Figure 6. With the initial guessed values $P^{(0)}=0$ except $P^{(0)}(1)=-0.1$, the target solution is arrived via three HB-AFT iterations.

Taking ω as a control parameter, periodic solutions of the system can be found by the HB-AFT scheme from 450 to 800 rad/s, and the corresponding Floquet multipliers are calculated as well. The stability of periodic solutions will be checked by using the leading Floquet multipliers that are the largest ones in absolute value among the Floquet multipliers calculated. In this way, the instable speed interval for a rotor system can be determined and controlled.

When $\omega=500$ rad/s, the periodic solution obtained by the HB-AFT scheme is (higher harmonic terms are omitted):

$$\begin{aligned} X &= -0.2157 + 0.1118 \cos(\tau) + 0.0044 \sin(\tau) \\ &\quad + 0.0526 \cos(2\tau) + 0.0087 \sin(2\tau) + 0.0187 \cos(3\tau) \\ &\quad + 0.0077 \sin(3\tau) + 0.0064 \cos(4\tau) + 0.0088 \sin(4\tau), \\ Y &= -0.0019 - 0.0059 \cos(\tau) + 0.1228 \sin(\tau) \\ &\quad - 0.0036 \cos(2\tau) + 0.0678 \sin(2\tau) - 0.0605 \cos(3\tau) \\ &\quad + 0.0879 \sin(3\tau) + 0.0020 \cos(4\tau) - 0.0140 \sin(4\tau). \end{aligned}$$

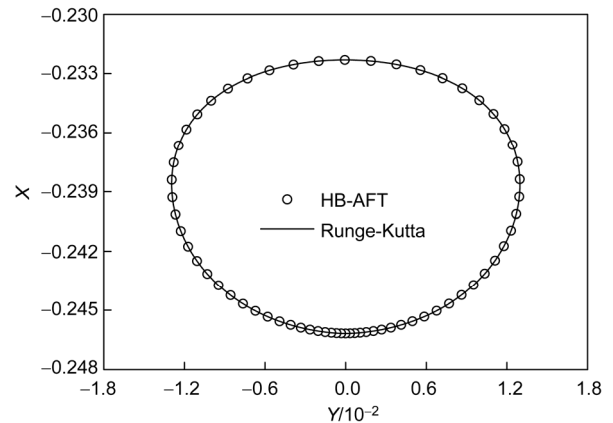


Figure 5 Axis orbit of the rotor at 150 rad/s.

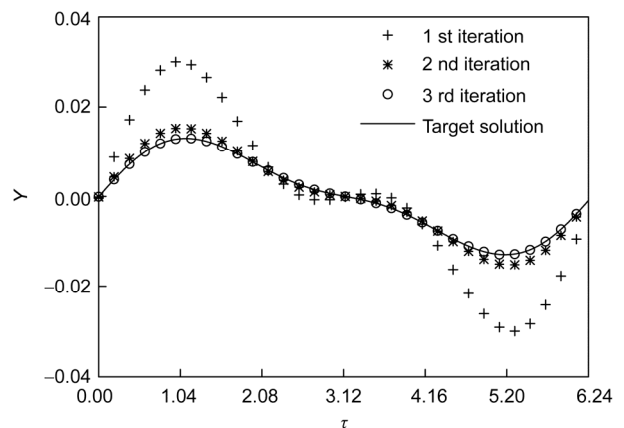


Figure 6 Convergence of the HB-AFT scheme.

and its leading Floquet multipliers calculated are $0.7160 \pm 0.4037i$ whose absolute value is equal to 0.8220 less than 1. Thus, the periodic motion is stable.

Comparisons of the HB-AFT scheme and Runge-Kutta method in phase portraits are shown in Figure 7, and the HB-AFT results agree well with the numerical simulation. Based on the numerical results obtained with Runge-Kutta method, spectrums of rotor response are also given in Figure 8 by FFT technique. It can be found that the first four order frequencies dominate the response of the system and thus the HB-AFT solution with eight order harmonic terms is accurate enough that is also confirmed by Figure 7. The coefficients of harmonic terms in X and Y match well with the magnitudes of frequencies shown in Figure 8. Moreover, the HB-AFT scheme facilitates saving of computation time because it is essentially a frequency-domain method.

Calculations indicate that two complex conjugate Floquet multipliers move out of the unit circle at 537 rad/s and then get back inside the unit circle at 547 rad/s. Thus the periodic solution will lose stability between 537 and 547 rad/s, and the secondary Hopf bifurcation occur. Table 1 gives the leading Floquet multipliers in detail and the varying process is illustrated in Figure 9(a). Calculations also point out that a real Floquet multiplier leaves the unit circle through -1 at 655 rad/s and then returns at 722 rad/s. Hence, the periodic solution is unstable from 655 to 722 rad/s, and the period-

doubling bifurcation occurs. The leading Floquet multipliers are given by Table 1 and illustrated in Figure 9(b).

To confirm the above results obtained with the HB-AFT scheme and Floquet theory, a numerical bifurcation diagram of the system is presented by Runge-Kutta method as shown in Figure 10. When the rotor runs from 450 to 537 rad/s, the periodic motion is stable and its attractor is a single point in Poincare map as shown in Figures 11(a) and 12(a). As rotor speed exceeds 537 rad/s, the periodic motion loses stability and the quasi-periodic motion appears as shown in Figure 11(b) and (c). The points of its attractor are separated into a closed curve in Poincare map as shown in Figure 12(b) and (c). This nonperiodic motion continues until the rotor speed reaches 547 rad/s and it returns to the periodic motion state.

The periodic motion remains stable when rotor runs from 547 to 655 rad/s. As rotor speed continues to increase, the period-2 motion occurs and two isolated points are seen in the Poincare map as shown in Figure 12(e) and (f). The period-2 motion lasts for a wide range of speed. When the rotor runs over 722 rad/s, the system goes back to periodic motion again. Therefore, the numerical simulation confirms the results obtained by HB-AFT scheme and Floquet theory.

To further confirm the feasibility of HB-AFT scheme, a numerical bifurcation diagram is calculated by Runge-Kutta method when the bearing clearance is set as zero as shown in Figure 13. Based on the HB-AFT scheme, the amplitude

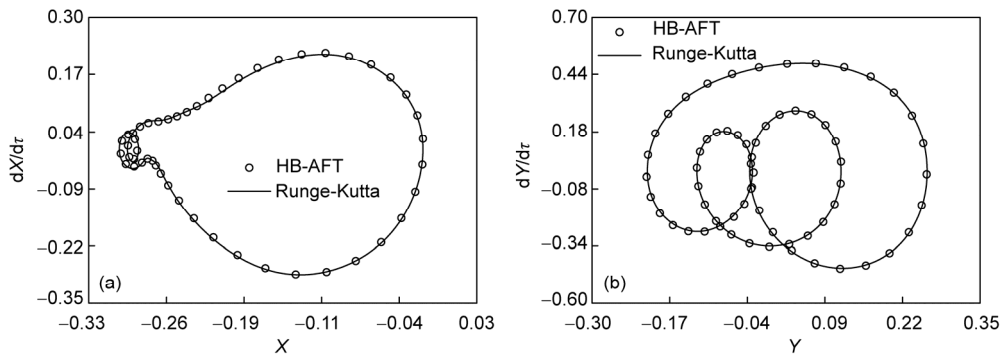


Figure 7 Phase portraits of the rotor response at 500 rad/s. (a) The phase portrait of X ; (b) the phase portrait of Y .

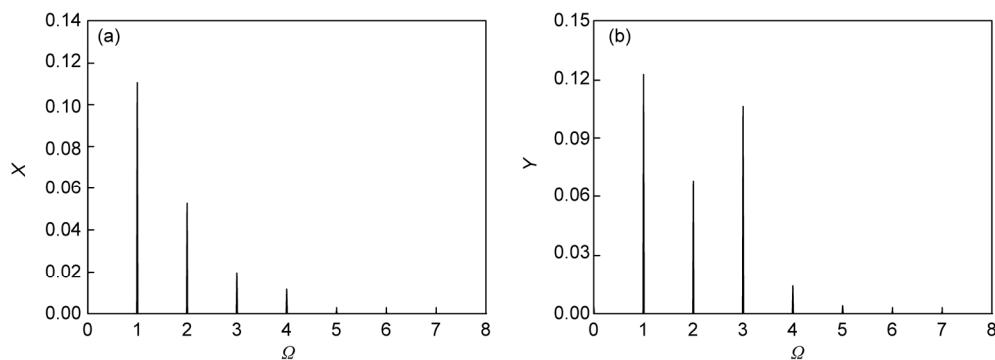


Figure 8 Spectrums of the rotor response at 500 rad/s. (a) The spectrum of X ; (b) the spectrum of Y .

Table 1 The leading Floquet multipliers at different rotor speeds

Rotor speed (rad/s)	Floquet multiplier	Absolute value
536	0.5369±0.7727i	0.9409
537	0.5537±0.8125i	0.9832
538	0.5668±0.8384i	1.0120
539	0.5773±0.8557i	1.0322
546	0.5966±0.8360i	1.0270
547	0.5897±0.8155i	1.0064
548	0.5785±0.7888i	0.9782
549	0.5601±0.7523i	0.9379
654	-0.9804	0.9804
655	-1.0045	1.0045
656	-1.0282	1.0282
657	-1.0538	1.0538
721	-1.0070	1.0070
722	-1.0010	1.0010
723	-0.9954	0.9954
724	-0.9899	0.9899

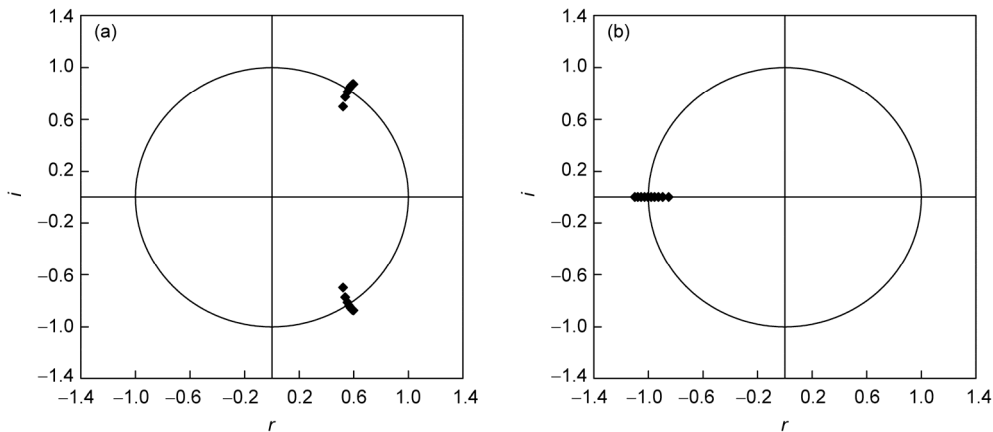


Figure 9 Illustration of the leading Floquet multipliers. (a) The Floquet multipliers around 537 rad/s; (b) the Floquet multipliers around 655 rad/s.

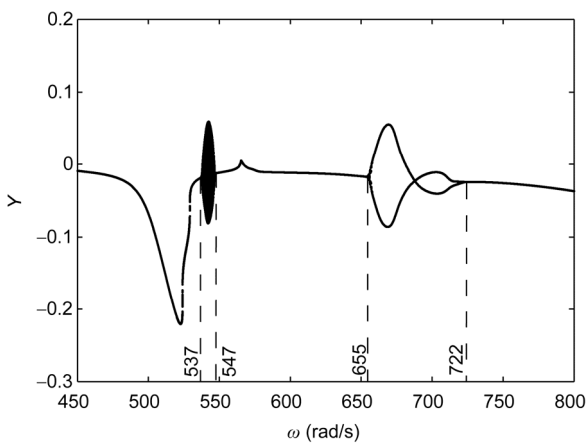


Figure 10 Bifurcation diagram with rotor speed as control parameter.

of each harmonic in periodic solution can also be obtained from 200 to 800 rad/s as shown in Figure 14. It should be noted that not all the periodic solutions are stable, and they will lose stability between 657 rad/s and 694 rad/s because of the period doubling bifurcation. Several resonance regions are found for higher order harmonics, and the third harmonic resonance located at 527 rad/s is the most obvious one among them. Of course, more resonance regions will be found in high speed interval, such as the primary resonance regions of rotor unbalance (the first harmonic) and coupling misalignment (the second harmonic) that are not discussed here due to space limitations. It can be observed that the HB AFT results keep consistent with the numerical simulation.

For the third harmonic resonance, comparisons between the HB-AFT results and numerical simulations are shown in Figure 15. Unlike the linear system, resonance curve leans

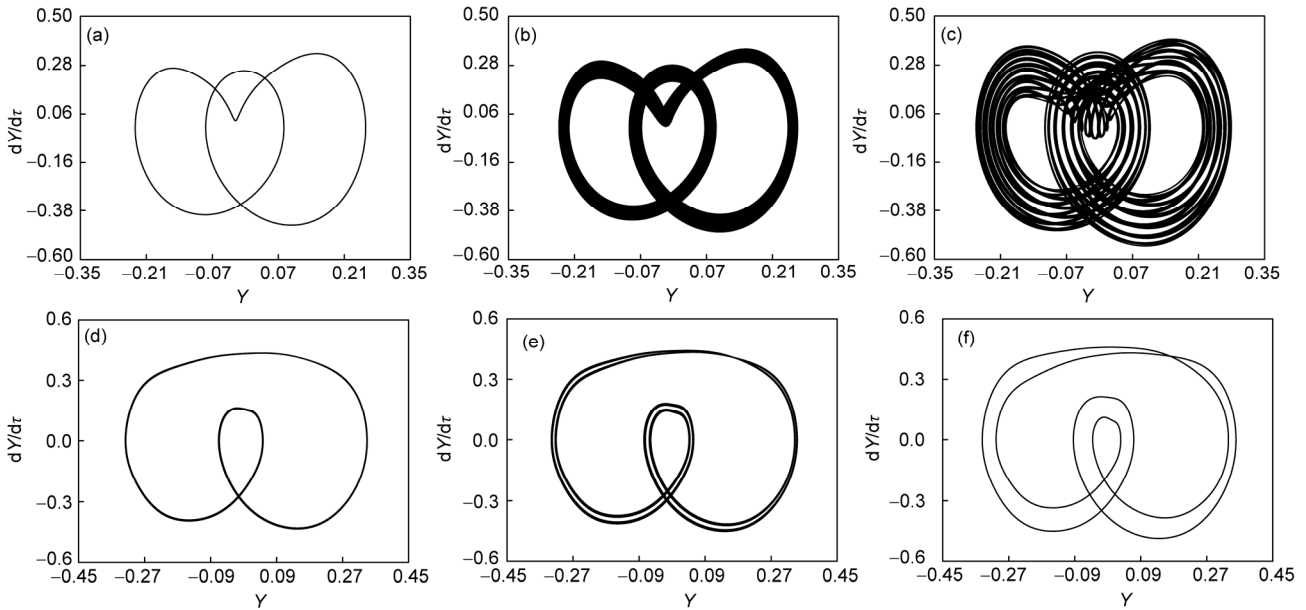


Figure 11 Phase portraits of Y at different rotor speeds. (a) Phase portrait at 537 rad/s; (b) phase portrait at 538 rad/s; (c) phase portrait at 539 rad/s; (d) phase portrait at 656 rad/s; (e) phase portrait at 657 rad/s; (f) the phase portrait at 658 rad/s.

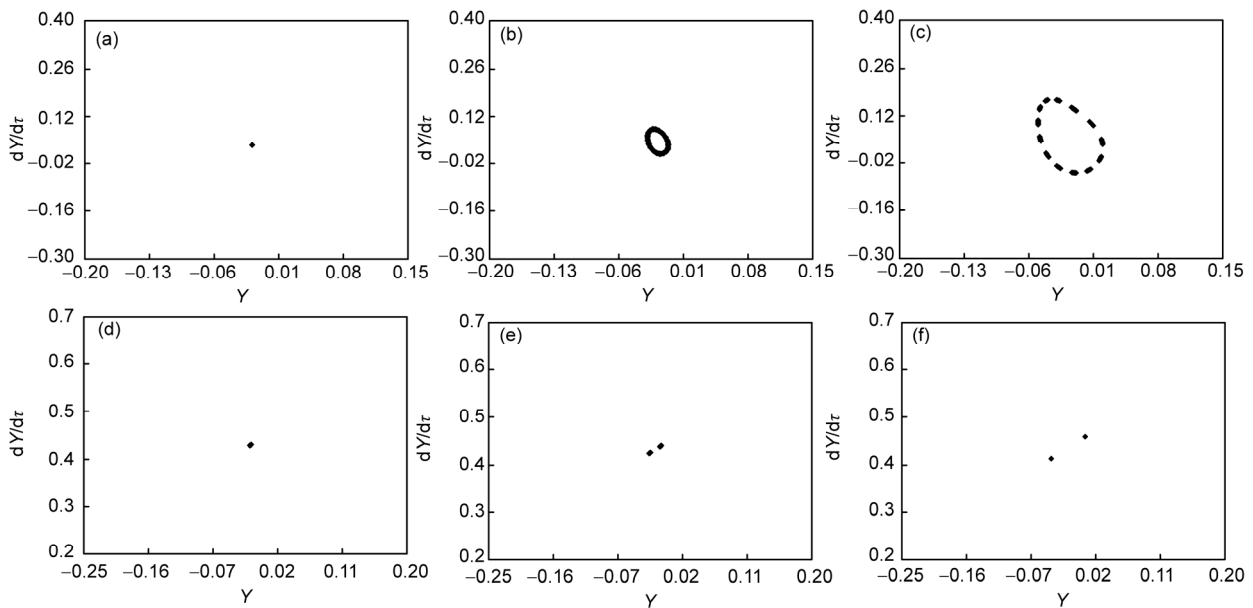


Figure 12 Poincare maps of Y at different rotor speeds. (a) Poincare map at 537 rad/s; (b) poincare map at 538 rad/s; (c) poincare map at 539 rad/s; (d) poincare map at 656 rad/s; (e) poincare map at 657 rad/s; (f) poincare map at 658 rad/s.

to the right with hard spring property that causes the jump and hysteresis phenomena. The two bold points A and B are actually the saddle-node bifurcation points, and the periodic solutions located on A-B branch are unstable. It can be seen that the numerical simulation confirms the HB-AFT results in Figure 15. Moreover, the resonance curves with different bearing parameters are also given by the HB-AFT scheme, as shown in Figure 16. It is indicated that bearing dampin can effectively suppress the peak value of resonance curve and prevent the jump behavior that is dangerous to the rotor

system. As bearing clearance increases, natural frequency of the system decreases and the rotor amplitude is enlarged.

5 Conclusion

The HB-AFT scheme is well-suited for solving strong non-linear problems, even the tough issues with both piecewise and irrational nonlinearities. Based on the HB-AFT scheme and the Floquet theory, a misaligned rotor system is focused

on and its periodic response properties are investigated. Two ways towards instability are found for periodic solutions in the different speed ranges. The secondary Hopf bifurcation occurs early and leads to the quasi-periodic motion. Later as the rotor runs up the period-doubling bifurcation occurs and lasts for a wide range of rotor speed. Finally, the numerical simulation confirms the results obtained with

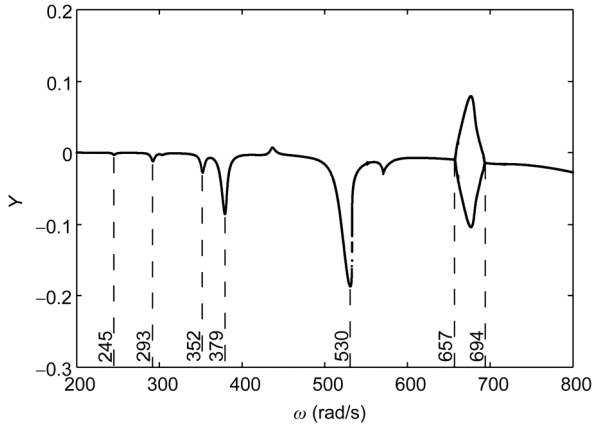


Figure 13 Bifurcation diagram with rotor speed as control parameter.

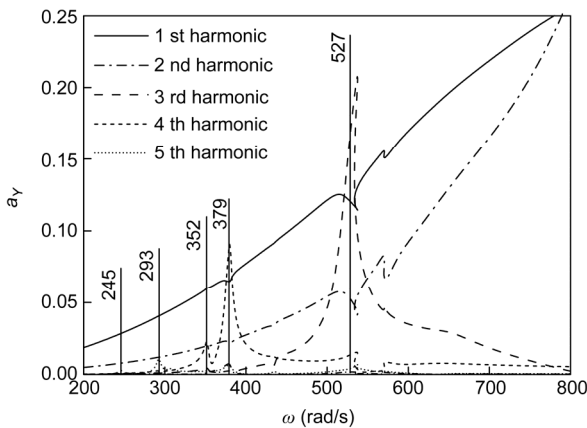


Figure 14 Amplitude of each harmonic varying with rotor speed.

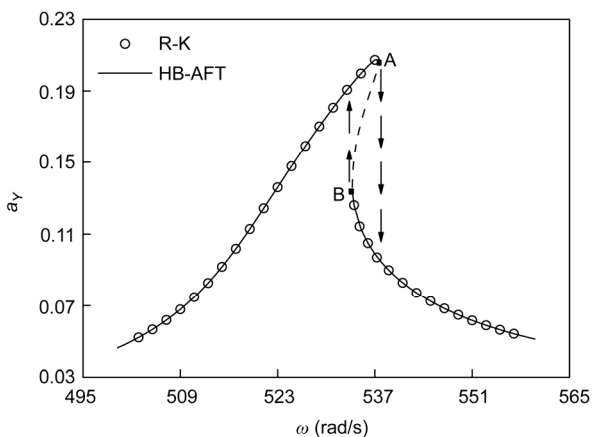


Figure 15 Comparisons of the HB-AFT and Runge-Kutta results.

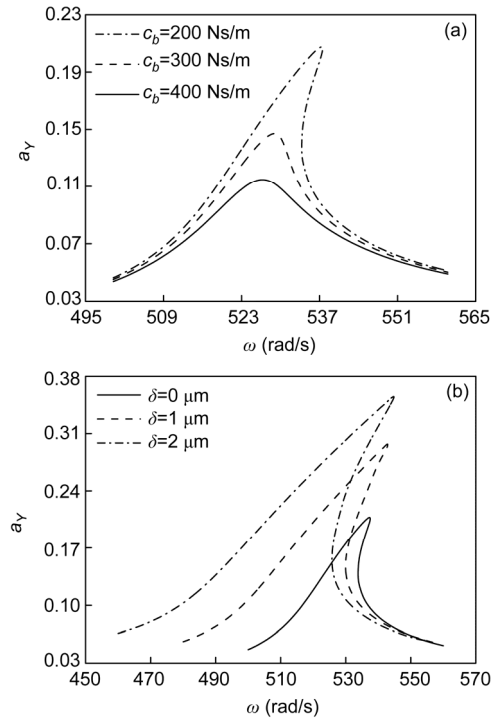


Figure 16 Resonance curves with different bearing parameters. (a) The resonance curves with different bearing damping; (b) the resonance curves with different bearing clearance.

the HB-AFT scheme and Floquet theory. Therefore, an effective way to estimate the dangerous speed range is presented, which may be significant for the global response analysis and dynamic optimal design of nonlinear rotor systems.

This work was supported by the National Basic Research Program of China ("973" Project) (Grant No. 2015CB057400), and the National Natural Science Foundation of China (Grant No. 11302058).

- 1 Dewell D L, Mitchell L D. Detection of a misaligned disk coupling using spectrum analysis. *ASME J Vib Acoust*, 1984, 106: 9–16
- 2 Sekhar A S, Prabhu B S. Effects of coupling misalignment on vibrations of rotating machinery. *J Sound Vib*, 1995, 185: 655–671
- 3 Xu M, Marangoni R D. Vibration analysis of a motor-flexible coupling-rotor system subject to misalignment and unbalance, Part I: theoretical model and analysis. *J Sound Vib*, 1994, 176: 663–679
- 4 Xu M, Marangoni R D. Vibration analysis of a motor-flexible coupling-rotor system subject to misalignment and unbalance, Part II: experimental validation. *J Sound Vib*, 1994, 176: 681–691
- 5 Lee Y S, Lee C W. Modelling and vibration analysis of misaligned rotor-ball bearing systems. *J Sound Vib*, 1999, 224: 17–32
- 6 Li M, Yu L. Analysis of the coupled lateral torsional vibration of a rotor-bearing system with a misaligned gear coupling. *J Sound Vib*, 2001, 243: 283–300
- 7 Al-Hussain K M, Redmond I. Dynamic response of two rotors connected by rigid mechanical coupling with parallel misalignment. *J Sound Vib*, 2002, 249: 483–498
- 8 Al-Hussain K M. Dynamic stability of two rigid rotors connected by a flexible coupling with angular misalignment. *J Sound Vib*, 2003, 266: 217–234
- 9 Sinha J K, Lees A W, Friswell M I. Estimating unbalance and misa-

- alignment of a flexible rotating machine from a single run-down. *J Sound Vib*, 2004, 272: 967–989
- 10 Lees A W. Misalignment in rigidly coupled rotors. *J Sound Vib*, 2007, 305: 261–271
- 11 Bouaziz S, Attia H M, Mataar M, et al. Dynamic behaviour of hydrodynamic journal bearings in presence of rotor spatial angular misalignment. *Mech Mach Theory*, 2009, 44: 1548–1559
- 12 Bouaziz S, Messaoud N B, Mataar M, et al. A theoretical model for analyzing the dynamic behavior of a misaligned rotor with active magnetic bearings. *Mechatronics*, 2011, 21: 899–907
- 13 Bouaziz S, Messaoud N B, Choley J Y, et al. Transient response of a rotor-AMBs system connected by a flexible mechanical coupling. *Mechatronics*, 2013, 23: 573–580
- 14 Patel T H, Darpe A K. Vibration response of misaligned rotors. *J Sound Vib*, 2009, 325: 609–628
- 15 Patel T H, Darpe A K. Experimental investigations on vibration response of misaligned rotors. *Mech Syst Signal Pr*, 2009, 23: 2236–2252
- 16 Jalan A K, Mohanty A R. Model based fault diagnosis of a rotor-bearing system for misalignment and unbalance under steady-state condition. *J Sound Vib*, 2009, 327: 604–622
- 17 Redmond I. Study of a misaligned flexibly coupled shaft system having nonlinear bearings and cyclic coupling stiffness—theoretical model and analysis. *J Sound Vib*, 2010, 329: 700–720
- 18 Rybczynski J. The possibility of evaluating turbo-set bearing misalignment defects on the basis of bearing trajectory features. *Mech Syst Signal Pr*, 2011, 25: 521–536
- 19 Lal M, Tiwari R. Multi-fault identification in simple rotor-bearing-coupling systems based on forced response measurements. *Mech Mach Theory*, 2012, 51: 87–109
- 20 Lal M, Tiwari R. Quantification of multiple fault parameters in flexible turbo-generator systems with incomplete rundown vibration data. *Mech Syst Signal Pr*, 2013, 41: 546–563
- 21 Lü J H, Chen G R. A time-varying complex dynamical network model and its controlled synchronization criteria. *IEEE T Autom Control*, 2005, 50: 841–846
- 22 Li Y, Wu X Q, Lu J A, et al. Synchronizability of duplex networks. *IEEE T Circuits-II*, 2016, 63: 206–210
- 23 Liu K X, Zhu H H, Lü J H. Bridging the gap between transmission noise and sampled data for robust consensus of multi-agent systems. *IEEE T Circuits-I*, 2015, 62: 1836–1844
- 24 Liu K X, Wu L L, Lü J H, et al. Finite-time adaptive consensus of a class of multi-agent systems. *Sci China Tech Sci*, 2016, 59: 22–32
- 25 Hou L, Chen Y S. Analysis of 1/2 sub-harmonic resonance in a maneuvering rotor system. *Sci China Tech Sci*, 2014, 57: 203–209
- 26 Hou L, Chen Y S. Super-harmonic responses analysis for a cracked rotor system considering inertial excitation. *Sci China Tech Sci*, 2015, 58: 1924–1934
- 27 Li D C, Xiang J W. Nonlinear aeroelastic analysis of airfoil using quasi-analytical approach (in Chinese). *Acta Aeronaut Astronaut Sin*, 2007, 28: 1080–1084
- 28 Niu Y B, Wang Z W. Flutter analysis of 2-D airfoil with nonlinearities using elliptic harmonic balance method (in Chinese). *Eng Mech*, 2013, 30: 461–465
- 29 Atadan A S, Huseyin K. An intrinsic method of harmonic analysis for nonlinear oscillations (a perturbation technique). *J Sound Vib*, 1984, 95: 525–530
- 30 Huseyin K, Lin R. An intrinsic multiple-scale harmonic balance method for nonlinear vibration and bifurcation problems. *Int J Nonlinear Mech*, 1991, 26: 727–740
- 31 Yuste S B. Comments on the method of harmonic balance in which Jacobi elliptic functions are used. *J Sound Vib*, 1991, 145: 381–390
- 32 Lau S L, Cheung Y K. Amplitude incremental variational principle for nonlinear vibration of elastic systems. *ASME J Appl Mech*, 1981, 48: 959–964
- 33 Liang F, Yang X D, Wen B C. Parametric resonances of clamped-clamped pipes conveying fluid by incremental harmonic balance method (in Chinese). *J Mech Eng*, 2009, 45: 126–130
- 34 Yan Z T, Zhang H F, Li Z L. Galloping analysis of iced transmission lines based on incremental harmonic balance method (in Chinese). *J Vib Eng*, 2012, 25: 161–166
- 35 Raghothama A, Narayanan S. Bifurcation and chaos in geared rotor bearing system by incremental harmonic balance method. *J Sound Vib*, 1999, 226: 469–492
- 36 Yang S P, Shen Y J, Liu X D. Nonlinear dynamics of gear system based on incremental harmonic balance method (in Chinese). *J Vib Shock*, 2005, 24: 40–42
- 37 Wang W, Song Y L, Li G X. Nonlinear dynamics of automobile steering using incremental harmonic balance method (in Chinese). *J Vib Eng*, 2010, 23: 355–360
- 38 Zhang J, Liu R Q, Guo H W, et al. Nonlinear dynamic characteristics of deployable structures with joints and cables based on incremental harmonic balance method (in Chinese). *J Vib Shock*, 2014, 33: 4–10
- 39 Cameron T M, Griffin J H. An alternating frequency/time domain method for calculating the steady-state response of nonlinear dynamic systems. *ASME J Appl Mech*, 1989, 56: 149–154
- 40 Yamauchi S. The nonlinear vibration of flexible rotors, 1st Report, Development of a new analysis technique. *Trans JSME C*, 1983, 49: 1862–1868
- 41 Kim Y B, Noah S T. Stability and bifurcation analysis of oscillators with piecewise-linear characteristics: A general approach. *ASME J Appl Mech*, 1991, 58: 545–553
- 42 Kim Y B, Noah S T. Response and bifurcation analysis of an MDOF rotor system with a strong nonlinearity. *Nonlinear Dyn*, 1991, 2: 215–234
- 43 Kim Y B, Noah S T. Quasi-periodic response and stability analysis for a non-linear Jeffcott rotor. *J Sound Vib*, 1996, 190: 239–253
- 44 Groll G V, Ewins D J. The harmonic balance method with arc-length continuation in rotor/stator contact problems. *J Sound Vib*, 2001, 241: 223–233
- 45 Tiwari M, Gupta K. Effect of radial internal clearance of a ball bearing on the dynamics of a balanced horizontal rotor. *J Sound Vib*, 2000, 238: 723–756
- 46 Villa C, Sinou J J, Thouverez F. Stability and vibration analysis of a complex flexible rotor bearing system. *Commun Nonlinear Sci Numer Simulat*, 2008, 13: 804–821
- 47 Zhang Z Y, Chen Y S, Li Z G. Influencing factors of the dynamic hysteresis in varying compliance vibrations of a ball bearing. *Sci China Tech Sci*, 2015, 58: 775–782
- 48 Zhang Z Y, Chen Y S, Cao Q J. Bifurcations and hysteresis of varying compliance vibrations in the primary parametric resonance for a ball bearing. *J Sound Vib*, 2015, 350: 171–184
- 49 Han J. Study on kinematic mechanism of misalignment fault of rotor system connected by gear coupling (in Chinese). *J Vib Eng*, 2004, 17: 416–420
- 50 Harsha S P, Sandeep K, Prakash R. Nonlinear dynamic response of a rotor bearing system due to surface waviness. *Nonlinear Dyn*, 2004, 37: 91–114
- 51 Saito S. Calculation of nonlinear unbalance response of horizontal Jeffcott rotors supported by ball bearings with radial clearances. *ASME J Vib Acoust*, 1985, 107: 416–420
- 52 Shen J H, Lin K C, Chen S H, et al. Bifurcation and route-to-chaos analyses for Mathieu-Duffing oscillator by the incremental harmonic balance method. *Nonlinear Dyn*, 2008, 52: 403–414